FEBS Letters 581 (2007) 5872–5878

X-ray structure of the PHF core C-terminus: Insight into the folding of the intrinsically disordered protein tau in Alzheimer's disease

Jozef Sevcik[a,b,c], Rostislav Skrabana[a,b], Radovan Dvorsky[d], Natalia Csokova[a,b], Khalid Iqbal[e], Michal Novak[a,*]

[a] *Institute of Neuroimmunology, Slovak Academy of Sciences, Dubravska cesta 9, 845 10 Bratislava, Slovakia*
[b] *Axon Neuroscience GmbH, Rennweg 95b, A-1030 Vienna, Austria*
[c] *Institute of Molecular Biology, Slovak Academy of Sciences, Dubravska cesta 21, 842 51 Bratislava, Slovakia*
[d] *Max Planck Institute for Molecular Physiology, Otto Hahn Strasse 11, 44227 Dortmund, Germany*
[e] *New York State Institute for Basic Research in Developmental Disabilities, Staten Island, NY 10314, USA*

Received 3 October 2007; revised 15 November 2007; accepted 19 November 2007

Available online 3 December 2007

Edited by Hans Eklund

Abstract **The major constituent of Alzheimer's disease paired helical filaments (PHF) core is intrinsically disordered protein (IDP) tau. In spite of a considerable effort, insoluble character of PHF together with inherent physical properties of IDP tau have precluded so far reconstruction of PHF 3D structure by X-ray crystallography or NMR spectroscopy. Here we present first crystallographic study of PHF core C-terminus. Using monoclonal antibody MN423 specific to the tertiary structure of the PHF core, the in vivo PHF structure was imprinted into recombinant core PHF tau. Crystallization of the complex led to determination of the structure of the core PHF tau protein fragment ^{386}TDHGAE^{391} at 1.65 Å resolution. Structural analysis suggests important role of the core PHF C-terminus for PHF assembly. It is reasonable to expect that this approach will help to reveal the structural principles underlying the tau protein assembly into PHF and possibly will facilitate rationale drug design for inhibition of Alzheimer neurofibrillary changes.**

Keywords: Tau protein; Folding after binding; Core PHF; Imprint; Mold; X-ray structure

1. Introduction

Tertiary structure dependent monoclonal antibodies are an important tool for investigation of the mechanism of pathological assembly of intrinsically disordered proteins (IDPs) [1,2]. Monoclonal antibody MN423 was raised against the paired helical filaments (PHF) core, protease resistant product of proteolytic cleavage of Alzheimer's PHF, which retains its characteristic morphological features and consists mainly of tau protein [3]. The MN423 has unequivocal specificity for tau ordered in the course of Alzheimer's disease into the PHF tau [4,5] and represents an in vivo imprint of the core PHF. The potential of MN423 in solving the core PHF tau structure was observed already in our first studies [3,6]. The epitope analysis revealed that three- and four-repeat tau isoforms are core constituents and allowed to determine the precise extent of 12 kDa, 93–95 amino acids long protease resistant tau unit of the core PHF [7,8]. Detailed analyzes showed that PHF core C-terminal pentapeptide ^{387}DHGAE^{391} is the main contributor to reactivity of MN423. For full reactivity a small contribution of PHF core N-terminal segments ^{306}VQIVYK^{311}, ^{321}KCGSL^{325} is required [9].

IDP tau has no defined structure [10]. However, it can undergo an induced folding or disorder-to-order transition when bound to its partner [11], which is in our study MN423. We have found that recombinant version of the core PHF tau showed the same binding properties as in vivo derived core PHF tau. Detailed examination of the binding mechanism suggests that recombinant core PHF tau undergoes folding transition during binding to MN423 – the core PHF mold. We have used this transition property of recombinant tau for crystallographic study of the core PHF tau. Here we describe the 3D structure of the PHF core C-terminus in the complex with MN423.

2. Materials and methods

2.1. Protein crystallization

Recombinant core PHF tau units tau306–391 and dGAE (tau297–391) were prepared as described previously [12]. MN423 Fab production, purification and preparation of two crystal forms (I and II) were described in [13]. From a number of co-crystallization trials with the complexes MN423–dGAE and MN423–tau306–391 only the later yielded well diffracting crystals. Crystals grew after 3 months from 3 μl drops containing equimolar amounts of MN423 Fab and recombinant tau306–391 mixed with precipitant solution in 1:1 ratio. The concentration of MN423 in 10 mM Tris–HCl, pH 7.2, with 50 mM NaCl was 10 mg/ml. As a precipitant solution 12% (w/v) PEG 3350 in 100 mM MES buffer, pH 7.0, etc. was used. The drop contained 1 mM DTT and 4 mM iodoacetamide.

2.2. Structure determination and refinement

X-ray data collection and processing was described previously [13]. All subsequent calculations were performed with programs from the CCP4 package [14] unless otherwise indicated. The structure was solved by molecular replacement with the program *MOLREP* [15] using as a search model randomly chosen Fab structure 1NBV [16]. The initial model yielded an *R*-factor of 52% and a correlation coefficient of 27% for data at 10–3 Å resolution. Molecular replacement

*Corresponding author. Fax: +421 2 54774276.
E-mail address: michal.novak@savba.sk (M. Novak).

Abbreviations: IDP, intrinsically disordered protein; PHF, paired helical filaments

0014-5793/$32.00
doi:10.1016/j.febslet.2007.11.067

showed clearly only one protein molecule in the asymmetric unit. The structure was refined with the maximum likelihood program *REFMAC5*, version 5.1.24 [17] against 95% of the data, the remaining 5% randomly excluded from the full data set by the program *UNIQUEIFY* were used for cross-validation in which R_{free}, the free R factor [18], was calculated to follow the progress of refinement. All data were included in the final refinement step. Refinement of the structure was altered with correcting the amino acid sequence and building the parts which were different from those of 1NBV. The models were inspected against $(3F_o - 2F_c, \alpha_c)$ and $(F_o - F_c, \alpha_c)$ maps and adjusted manually between the cycles of refinement with the program *XtalView* [19]. After each refinement cycle, the automated refinement procedure *ARP/wARP* [20] was applied for modeling and updating the solvent structure. The structure was initially refined with isotropic, and in the later stages after the R factor had fallen to about 25%, with anisotropic temperature factors including the contributions to the structure factors from the hydrogen atoms. Hydrogen atoms were generated according to established geometrical criteria on their parent C, N and O atoms. The temperature factors of the hydrogen atoms were set equal to those of their parent atom. The inclusion of hydrogen atoms lowered the values of R and R_{free} by more than one unit. Isotropic and anisotropic temperature factors, bond lengths, and bond angles were restrained according to the standard criteria employed by *REFMAC*. Occupancies of water molecules were set to unity and not refined. When the refinement converged with R and R_{free} factors of 16.5% and 22.0%, respectively, the residues forming the core PHF tau fragment were included into the PDB file. Next few refinement cycles converged with final R and R_{free} of 16.0% and 21.8%, respectively. The refinement statistics are in Table 2. Atomic coordinates and diffraction data for the complex of monoclonal antibody MN423 with the core PHF tau fragment have been deposited in the Protein Data Bank, http://www.pdb.org (PDB ID code 2v17).

2.3. Docking of the core PHF tau C-terminal fragment into MN423 binding site

Structure of monoclonal antibody MN423 Fab fragment was imported into the molecular modeling program Sybyl (Tripos Inc., St. Louis, MO, USA; http://www.tripos.com) and all water molecules were removed. Hydrogen atoms were remodeled using Sybyl Biopolymer module. Amino-terminal and carboxy-terminal groups were set to be protonated and deprotonated, respectively. Steric clashes caused by added atoms were removed by 100 cycles of minimization of protein energy. Model of C-terminal pentapeptide ^{387}DHGAE^{391} of the core PHF tau protein with acetylated N-terminus was created with the help of Sybyl Biopolymer module. Carboxy-terminal group was considered as deprotonated. The antibody binding site was defined according to MacCallum et al. [21] with origin of the binding site at the average position of Arg30L, Lys31L, Arg52H and Lys56H. A radius of 20 Å from the origin was used to define the active site of the protein. 100 independent dockings of peptide to the active site were performed using the program GOLD version 3.0 [22]. Default parameters of genetic algorithm were used for each docking: a maximum number of 100 000 operations were performed on a population of 100 individuals with a selection pressure of 1.1; operator weights for crossover, mutation, and migration were set to 95, 95 and 10, respectively. GOLD fitness function was finally used to evaluate the accuracy of binding modes. From these one pose was chosen on the basis of scoring fitness value (85.04 in overall rating), geometrical fit and chemical acceptance of contacts.

2.4. Surface plasmon resonance measurements

BIACORE3000 instrument with CM5 sensorchip (Biacore AB, Uppsala) was used. Amine-coupling reagents (EDC, NHS, ethanolamine pH 8.5), P20 detergent and 10 mM sodium acetate pH 5.0 were obtained from Biacore AB. All experiments were performed at 25 °C in phosphate-buffered saline pH 7.4 with 0.005% of P20 (PBS-P) as the running buffer. Typically, 5000 RU (response units) of polyclonal anti-mouse antibody (No. Z 0420; DakoCytomation, Glostrup, Denmark) was coupled at pH 5.0 via primary amines simultaneously in two flow cells, one of which was used as a reference in measurement. In each analysis cycle, MN423 (5 μg/ml in PBS-P) was captured in the analytical flow cell to reach immobilization level 230–250 RU. For determination of reaction mechanism, 330 nM solution of the recombinant core PHF tau unit dGAE was layered on sensorchip for 1, 3 and 20 min at 10 μl/min flow rate and its dissociation was recorded for another 15 min. The ends of injection on the sensorgrams were aligned and overlaid. For K_D determination, duplicates of two-fold serial dilutions of dGAE (5–80 nM) and three-fold serial dilutions of tau306–391 (6–150 nM), including PBS-P as a control, were injected at a flow rate 50 μl/min over the sensorchip, with 3 and 7 min of association and dissociation time, respectively. Kinetic binding data were double referenced [23] and fitted by BIA evaluation software 4.1 (Biacore AB) to two-phase reaction model. Kinetic rate constants were approximated globally, maximal responses were fitted locally and bulk response was set to zero.

3. Results

3.1. MN423 core PHF imprint is a mold for recombinant IDP tau

It has been shown by immunoblotting that MN423 recognizes recombinant core PHF unit dGAE (tau297–391) with an equal affinity as the genuine PHF core [8]. A quantitative ELISA study revealed that MN423 epitope determinants on the PHF core comprise spatial cooperation of C-terminal pentapeptide ^{387}DHGAE^{391} with two N-terminal segments ^{306}VQIVYK^{311} and ^{321}KCGSL^{325} [8,9] suggesting that MN423 induces a conformational rearrangement and folding of IDP tau. To confirm this assumption, we examined the mechanism of complex formation between the MN423 and recombinant PHF core tau represented by dGAE. Surface plasmon resonance analysis revealed two-phase interaction consisting of the fast initial phase, followed by a slower phase which further contributes to the complex stability by decreasing dissociation rate (Fig. 1A). The second slow interaction phase reflects structural rearrangement of dGAE unit in the course of binding. Further, we determined K_D of complexes of MN423 with core PHF tau units dGAE and tau306–391 applying two-phase reaction mechanism. Good fit was obtained yielding similar affinity for both units (Fig. 1B and C). It could be concluded that intrinsically disordered recombinant core PHF tau units, when exposed to interaction with PHF core imprint – MN423, acquire an in vivo PHF core fold and that the MN423 serves as a mold aiding the transition of IDP tau into specific ordered state.

3.2. Structure of the core PHF tau imprint – MN423 Fab fragment

Having confirmed the presence of a PHF core-like fold in the complex of MN423 with recombinant PHF core tau units, we aimed at crystallographic determination of its structure. The structure was solved by molecular replacement and refined to R/R_{free} values of 16.0%/21.8%. There is one molecule of the Fab fragment of monoclonal antibody MN423 in the asymmetric unit consisting of 214 (light-chain) and 225 (heavy-chain) residues. Due to the lack of reasonably clear electron density, the C-terminal residues Gly223H–Pro224H–Ile225H were not modeled. The main secondary structure elements of the Fab fragment are β-strands with only two short α-helices in the light chain (Fig. 2). The elbow angle corresponding to the pseudodyad axis between the Fab constant and variable domains is 165°. This value is within the minimum of bimodal elbow angle distribution observed for Fab fragments [24]. The angle was calculated by web-based service RBOW (http://as2ts.llnl.gov/AS2TS/RBOW). The final model contains 1672 and 1651 non-hydrogen atoms in L and H chain, respectively,

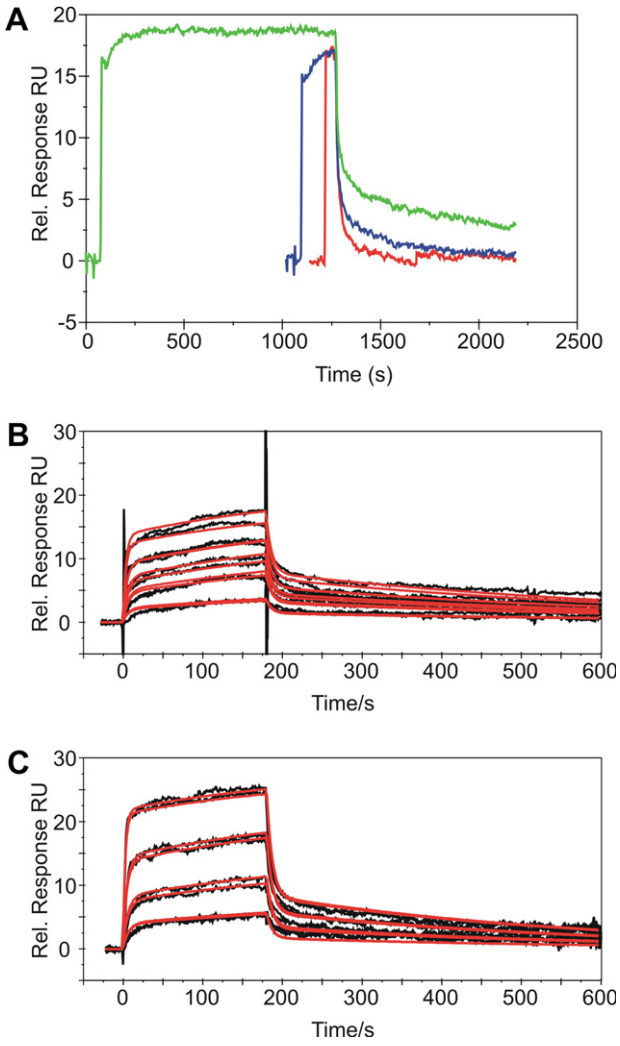

Fig. 1. Two-phase binding of the recombinant core PHF tau units to MN423. (A) dGAE was injected over MN423 surface with three different contact times (red – 1 min, blue – 3 min, green – 20 min) and its dissociation was followed for 15 min. Stability of the complex increased in direct proportion to the contact time suggesting two-phase reaction mechanism: first phase characterized by fast association and fast dissociation and concomitant second phase in which additional contacts between dGAE and MN423 were created, contributing to decrease of dissociation rate of the complex. RU – response unit. (B and C) Two-phase interaction model was used for K_D determination of MN423–dGAE (B) and MN423–tau306–391 (C) complexes. Calculated fits of sensorgrams (red lines) show excellent agreement with experimental data. The association and dissociation rate constants k_a and k_d, respectively, are as follows: dGAE – first phase $k_a = 1.8 \times 10^6 \pm 5.5 \times 10^4\ s^{-1}\ M^{-1}$, $k_d = 1.4 \times 10^{-1} \pm 2.7 \times 10^{-3}\ s^{-1}$; second phase $k_a = 4.3 \times 10^{-3} \pm 4.4 \times 10^{-5}\ s^{-1}\ M^{-1}$, $k_d = 2.0 \times 10^{-3} \pm 3.2 \times 10^{-5}\ s^{-1}$; $K_D = 24$ nM; tau306–391 – first phase $k_a = 1.4 \times 10^6 \pm 3.4 \times 10^4\ s^{-1}\ M^{-1}$, $k_d = 1.4 \times 10^{-1} \pm 2.0 \times 10^{-3}\ s^{-1}$; second phase $k_a = 2.9 \times 10^{-3} \pm 2.9 \times 10^{-5}\ s^{-1}\ M^{-1}$, $k_d = 2.5 \times 10^{-3} \pm 3.5 \times 10^{-5}\ s^{-1}$; $K_D = 46$ nM.

44 atoms of the core PHF unit fragment and 702 water molecules. There are 11 proline residues in the light and 13 in the heavy-chain. Five of these, namely Pro8L, Pro95L, Pro141L, Pro156H and Pro198H, and two serine residues, Ser158H and Ser165H have the preceding peptide bond in *cis* conformation. The protein contains five cysteine residues in both the light- and the heavy-chain. In each chain there are two S–S bridges: Cys23L–Cys88L, Cys134L–Cys194L, and Cys22H–Cys98H, Cys149H–Cys204H. Cys23L was modeled with two conformations of SH group, each forming S–S bridge with its partner. There are two unpaired cysteine residues, C-terminal residue Cys214L and Cys137H located in a flexible surface loop. The two cysteine residues do not occupy typical conformation required for S–S bridge. The distance of their CA atoms is only 4.82 Å, which is too short to allow formation of the bridge. Under physiological conditions these two cysteine residues form a disulfide bond [13]. Breaking of the Cys214L–Cys137H bridge is very likely caused by the presence of DTT in crystallizing solution. As a consequence, the two interacting loops are destabilized, having *B*-factor values about three-times higher than the average (Fig. 3). As confirmed by ELISA (data not shown), 1 mM DTT used in crystallization solution did not decrease stability of the complex MN423–tau306–391. It is not surprising, as the cysteines under discussion are far apart from the binding site (Fig. 2). The model contains a large number of water molecules (702). Out of these only 14 have *B* factor greater than 50 Å^2. These were checked in electron density (>0.5σ) and as they satisfied all criteria for water molecules were not removed from the final model. Thermal parameters of this magnitude are physically reasonable as water molecules are only weakly held by H-bonding contacts and are able to vibrate considerably or may not be fully occupied.

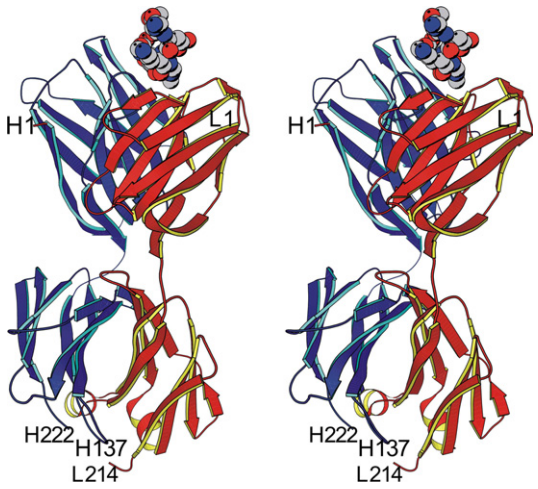

Fig. 2. Stereo picture of the structure of MN423 Fab fragment (ribbon diagram) with the core PHF tau C-terminal residues ^{388}TDHGAE^{391} (space filling model) located in the antibody binding site. Chain L is in red, H in blue. The figure was drawn by the program *MOLSCRIPT* [40].

3.3. Structure of the PHF core C-terminus and its binding to MN423

Due to the long time required for crystal growth and high susceptibility of recombinant tau to proteolysis, the proteins from crystal used for data collection were analyzed by silver-stained SDS–PAGE and immunoblotting. As tau306–391 has not been found in the crystal (data not shown), it is likely that it was digested during crystallization by an endoproteolytic activity present in the crystallization drop. It is why the structure of only MN423 Fab fragment was refined. In parallel, the PHF core C-terminal pentapeptide ^{387}DHGAE^{391}, which constitutes the minimal recognition site of MN423 with the affinity

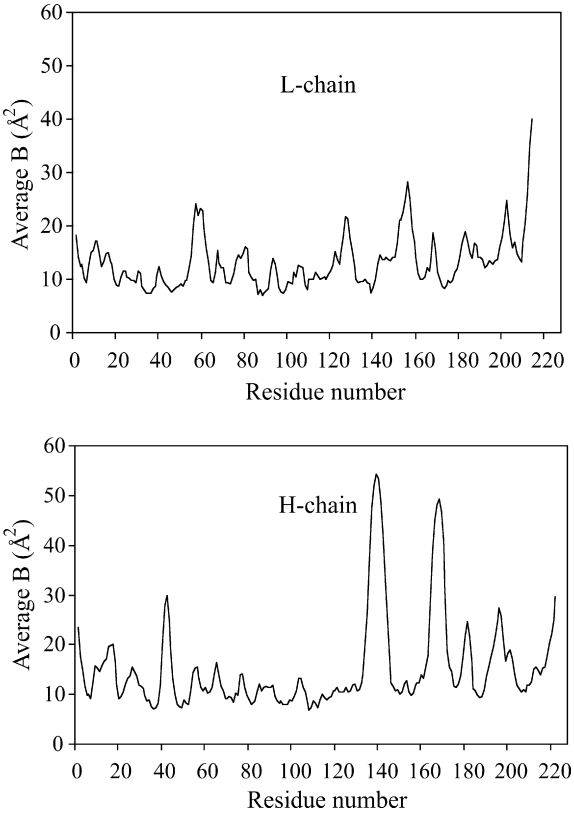

Fig. 3. Distribution of the main-chain average B values along the light- and heavy-chain of the MN423 Fab fragment as a function of residue numbers. Note the highly destabilized C-terminus of the light-chain and two flexible loops in the constant region of the heavy-chain. Destabilization of the C-terminal L region and the loop around residue 140 in the heavy-chain is caused by Cys214L–Cys137H bridge reduction. The residues 165H–171H form a surface loop protruding from the protein without any stabilizing contacts to the molecule which explains its high flexibility.

in micromolar range [25], was docked into the binding site of MN423. Surprisingly, at the end of MN423 structure refinement there was clear difference electron density at the binding site which corresponded well to the position of in silico modeled pentapeptide ^{387}DHGAE^{391} (Fig. 4A). Further refinement and rebuilding of the pentapeptide gave a unique structure with an excellent fit to the electron density, suggesting full occupancy and allowing to build-in also the sixth residue Thr386 (Fig. 4B). Inclusion of the peptide improved refinement statistics (see above). PHF core C-terminal hexapeptide ^{386}TDHGAE^{391} has a form of a loop, which is not stabilized by any direct intrachain hydrogen bonds (Fig. 4B). The surface area of the hexapeptide is 829 Å^2, approximately one-half of it (421 Å^2) is buried in the binding site showing high shape and charge complementarity (Fig. 4C). The core fragment makes seven direct and five water mediated hydrogen bonds with MN423 (Fig. 4D and Table 1). The C-terminal main-chain carboxyl of Glu391A of tau fragment, which was previously shown to be indispensable for the MN423 recognition [8,26], forms four H-bonds: two with Arg52H and one with Tyr33H and Tyr94L. The Asp387A side-chain carboxyl has been shown to confer the ultimate contribution to the affinity of the C-terminus of the core PHF tau [25], it forms two H-bonds with Arg30L. To the binding affinity contributes also H-bond between Ala390A main-chain nitrogen and Tyr94L main-chain oxygen as well as H-bonds mediated through water molecules. Dense packing of amino acids around Gly389A, the CA atom of which is directly facing the aromatic ring of Phe32L (Fig. 5), does not allow any amino acid but glycine to occupy this position. It is structural confirmation of our previous observation on absolute requirement for Gly at the −3 position for MN423 recognition [26].

3.4. Accuracy of the model

Electron density was clear throughout the whole structure except for a few flexible surface loops with highest B values. These can be identified from the plot of average B values of the main-chain atoms as a function of residue numbers (Fig. 3). Estimated standard uncertainty (ESU) based on R and R_{free} factors (the Cruickshank's dispersion precision indicator DPI, [27]) and the average temperature factors for protein atoms and water molecules are shown in Table 2. The temperature factors are in good agreement with the estimates from the Wilson plot [28]. The Ramachandran plot [29] calculated by the program PROCHECK [30] for the structure shows that there are 90.4% in the L chain and 91.0% in the H chain of residues in the most favored regions. The reminders are in the additionally allowed regions except Arg30L and Ser165H, the torsion angles of which are in generously allowed region. Inspection of the electron density around Arg30L, which is very clear, does not show any indication of errors in placing the main-chain atoms. Ser165H is in the flexible surface loop which might have caused deviations of its torsion angles from ideal values. The ω angle deviates from planarity for most of residues in the model. For some residues ω deviates by as much as 20°. This agrees with observations in a number of very accurate atomic resolution structures [31–33]. The average value for ω angle is 178.0° and 178.4° with standard deviations of 6.4° and 7.3° for L and H chains, respectively.

4. Discussion

This work represents the first crystallographic insight into the intrinsically disordered protein tau in Alzheimer's disease core PHF. There are a number of laboratories struggling to determine the structure of the core PHF tau. Each laboratory has developed its own methodology and the use of different techniques, as circular dichroism, nuclear magnetic resonance, X-ray diffraction and some others. There have been suggested several models of the arrangement of tau molecules within the PHFs or in solution (e.g. [34–38] and others). In spite of that the structure of tau still escapes its determination.

MN423 is the core PHF-specific antibody representing 3D imprint of the in vivo PHF tertiary structure. As it reacts with recombinant version of the core PHF tau in similar way as with in vivo derived core PHF tau, it is reasonable to say that MN423 represents a PHF core mold for recombinant tau. The C-terminal hexapeptide of the compact PHF core was fixed in the MN423 binding site and its structure was determined. As the MN423 was raised against a compact, protease resistant core PHF tau [3,5], the hexapeptide directly interacting with MN423 is an integral part of the compact PHF core. The loop conformation of the hexapeptide ^{386}TDHGAE^{391}, described in this study thus represents the genuine structure of core PHF tau C-terminus. Notwithstanding the hexapeptide lies outside

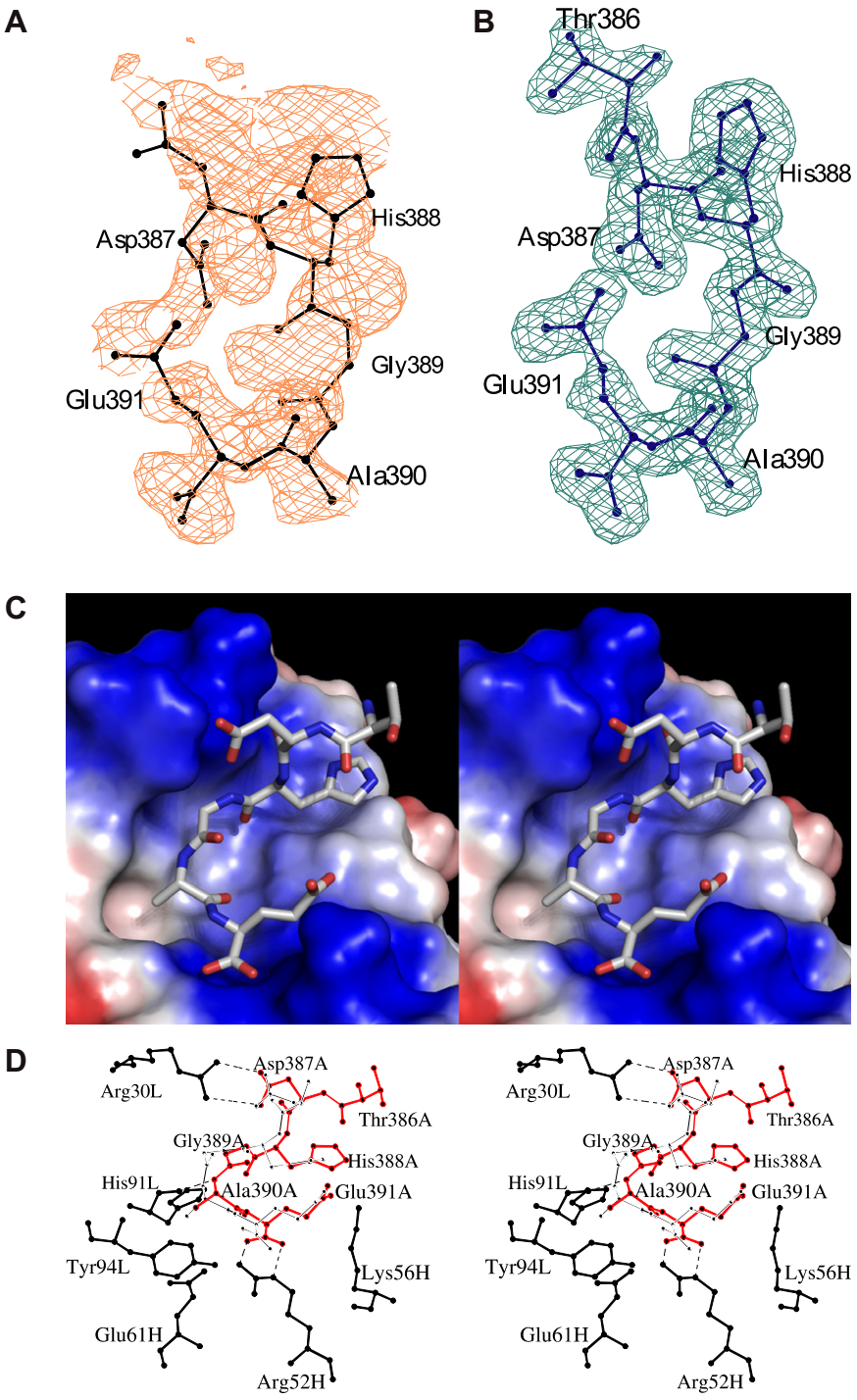

Fig. 4. Structure of the C-terminal hexapeptide ^{387}TDHGAE^{391} of PHF core and its binding by antibody MN423. (A) Difference electron density (1σ) at the binding site of antibody MN423 and in silico modeled pentapeptide ^{387}DHGAE^{391} with acetylated N-terminus before the residues were included in the refinement. (B) Electron density and the model of hexapeptide ^{387}TDHGAE^{391} after refinement. (C) The core PHF fragment in the binding site of the antibody MN423 (in stereo) shows shape and charge fit. The molecular surface is colored by electrostatic potential isocontours (blue +71.5 kT/e; red –71.5 kT/e). (D) Detailed stereoview on the core PHF tau C-terminal segment (chain A, in red) and the surrounding residues of the antibody (black) with the most important direct H-bonds (dashed lines). The conformation of the docked pentapeptide, drawn in light black, is close to that determined by X-rays. The figures (A) and (B) were drawn by the program *BOBSCRIPT* [41], the figure (C) was prepared by the program *PYMOL* (http://pymol.sourceforge.net) with surface electrostatic potential calculated by APBS [42] in the *PYMOL*, the figure (D) was drawn by the program *MOLSCRIPT* [40].

the repeat region known to convert to beta-structure during PHF assembly [39], its close association with the compact PHF core suggests a potential role of the C-terminal core peptide in PHF assembly.

Table 1
Direct and water mediated hydrogen bonds between MN423 and the ligand

Atom	Distance (Å)	Atom	Distance (Å)	Atom
His91L O	2.88	Ala390A N		
Arg52H NE	2.80	Glu391A OT		
Tyr33H OH	2.62	Glu391A OT		
Arg52H NH2	2.88	Glu391A O		
Tyr94L OH	2.72	Glu391A O		
Arg30L NH1	3.52	Asp387A OD1		
Arg30L NH2	2.77	Asp387A OD2		
His91L ND1	2.99	W3	2.82	Ala390A O
Arg106H N	2.94	W20	2.81	Ala390A O
		W20	3.50	Glu391A OE2
Ala107H N	3.19	W3	2.76	His388A O
Ser50L OG	2.75	W117	2.63	His388A ND1

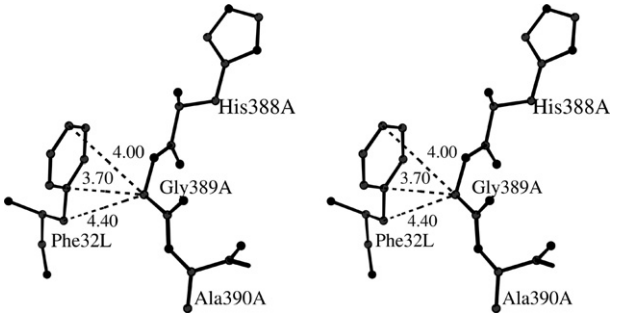

Fig. 5. A detailed view on Gly389A interaction with Phe32L (in stereo) shows dense packing of the two residues which does not allow any other amino acid but glycine to occupy this position. The figure was drawn by the program *MOLSCRIPT* [40].

The structure of the complex was solved by molecular replacement and refined with high accuracy to R/R_{free} factors of 16%/22% at a resolution of 1.65 Å. In the Protein Data Bank there have been deposited more than 500 structures of antibody Fab fragments, less than 20 of them with resolution better than 1.65 Å and comparable accuracy. Geometry of the structure is very good as judged by Ramachandran plot. The core PHF tau fragment ^{386}TDHGAE^{391} is positioned in a cavity formed by hypervariable loops of L and H chain making a number of contacts with the protein. Differences between coordinates of the core PHF tau peptide found by docking and those in the final model were small. Structure of the complex is in perfect agreement with the previously published biochemical data [8,9,25,26], which independently confirm correctness of the peptide structure.

The approach presented here suggests a new possibility in crystallographic analysis of intrinsically disordered proteins involved in pathogenesis of neurodegenerative diseases. Presented structure of PHF core C-terminal hexapeptide confirmed known property of IDPs to undergo disorder-to-order transition when they interact with binding partners. The PHF core imprint, monoclonal antibody MN423 serves as a mold for a part of recombinant tau which after induced folding acquires the same conformation as the core PHF. We are aware of the fact that proposed approach probably cannot solve the structure of the core PHF as a whole but by parts, if other conformation-dependent monoclonals could be prepared. In combination with in silico docking aimed at finding a physically feasible binding mode, it may represent a powerful tool for structural studies of IDP tau.

Table 2
Refinement statistics

Space group	$P2_1$
Unit cell	
a (Å)	71.54
b (Å)	36.81
c (Å)	85.54
β (°)	113.93
Protein molecules in asymmetric unit	1
Resolution (Å)	1.65
R (%)[a]	16.0
R_{free} (%)[b]	21.8
Model – atom sites	3323
Ligand – atom sites	44
Solvent molecules	702
Average B values (Å²)	
Protein atoms L/H	14.4/15.5
Ligand	21.4
Solvent molecules	29.6
B (Wilson plot) (Å²)	12.81
Coordinates ESU based on R/R_{free} (Å)	0.165/0.108
ESU based on maximum likelihood (Å)	0.064
Stereochemical restraints, r.m.s. (σ)	
Bond lengths (Å)	0.016
Bond angles (°)	1.663
Chiral centers (Å³)	0.182
Planar groups (Å)	0.008
B factors restraints (Å²)	
Main-chain bond	1.311
Main-chain angle	2.218
Side-chain bond	2.937
Side-chain angle	4.267

[a] $R = \sum|F_o - F_c|/\sum|F_o|$, where F_o and F_c are the observed and calculated structure factors.
[b] R_{free} was calculated as *R* but only for 5% of data.

Acknowledgments: This work was supported by Axon Neuroscience and partially by the Slovak Grant Agency VEGA Grants 2/4044/26 (J.S.) and 2/6091/26 (N.C.), by the International Centre for Genetic Engineering and Biotechnology Grant CRP/SVK05-01 (J.S., R.S. and N.C.) and by the Slovak Research and Development Agency under the Contract No. APVV-0471-06 (J.S. and R.S.). For access to DESY EMBL Hamburg Outstation, we acknowledge the support of the European Community Research Infrastructure Action under the FP6 "Structuring the European Research Area Specific Programme", Contract Number RII3-CT-2004-506008. We thank the Slovak Biotechnology Centre of Excellence (BITCET) for using the BIACORE 3000 instrument.

References

[1] Glabe, C.G. (2004) Conformation-dependent antibodies target diseases of protein misfolding. Trends Biochem. Sci. 29, 542–547.
[2] Skrabana, R., Sevcik, J. and Novak, M. (2006) Intrinsically disordered proteins in the neurodegenerative processes: formation of tau protein paired helical filaments and their analysis. Cell. Mol. Neurobiol. 26, 1085–1097.
[3] Novak, M., Wischik, C.M., Edwards, P., Pannell, R. and Milstein, C. (1989) Characterisation of the first monoclonal antibody against the pronase resistant core of the Alzheimer PHF. Prog. Clin. Biol. Res. 317, 755–761.
[4] Wischik, C.M., Novak, M., Edwards, P.C., Klug, A., Tichelaar, W. and Crowther, R.A. (1988) Structural characterization of the core of the paired helical filament of Alzheimer disease. Proc. Natl. Acad. Sci. U.S.A. 85, 4884–4888.

[5] Wischik, C.M. et al. (1988) Isolation of a fragment of tau derived from the core of the Paired Helical Filament of Alzheimer disease. Proc. Natl. Acad. Sci. U.S.A. 85, 4506–4510.
[6] Novak, M., Jakes, R., Edwards, P.C., Milstein, C. and Wischik, C.M. (1991) Difference between the tau protein of Alzheimer Paired Helical Filament core and normal tau revealed by epitope analysis of monoclonal antibodies 423 and 7.51. Proc. Natl. Acad. Sci. U.S.A. 88, 5837–5841.
[7] Jakes, R., Novak, M., Davison, M. and Wischik, C.M. (1991) Identification of 3- and 4-repeat tau isoforms within the PHF in Alzheimer's disease. EMBO J. 10, 2725–2729.
[8] Novak, M., Kabat, J. and Wischik, C.M. (1993) Molecular characterization of the minimal protease resistant tau unit of the Alzheimer's disease Paired Helical Filament. EMBO J. 12, 365–370.
[9] Skrabana, R., Kontsek, P., Mederlyova, A., Iqbal, K. and Novak, M. (2004) Folding of Alzheimer's core PHF subunit revealed by monoclonal antibody 423. FEBS Lett. 568, 178–182.
[10] Uversky, V.N. (2002) Natively unfolded proteins: a point where biology waits for physics. Protein Sci. 11, 739–756.
[11] Dyson, H.J. and Wright, P.E. (2005) Intrinsically unstructured proteins and their functions. Nat. Rev. Mol. Cell. Biol. 6, 197–208.
[12] Csokova, N., Skrabana, R., Liebig, H.D., Mederlyova, A., Kontsek, P. and Novak, M. (2004) Rapid purification of truncated tau proteins: model approach to purification of functionally active fragments of disordered proteins, implication for neurodegenerative diseases. Protein Expres. Purif. 35, 366–372.
[13] Csokova, N., Skrabana, R., Urbanikova, L., Kovacech, B., Popov, A., Sevcik, J. and Novak, M. (2006) Preparation, crystallization and preliminary X-ray analysis of the Fab fragment of monoclonal antibody MN423, revealing the structural aspects of Alzheimer's paired helical filaments. Protein Peptide Lett. 13, 941–944.
[14] CCP4 (1994) The CCP4 suite: programs for protein crystallography. Acta Crystallogr. D: Biol. Crystallogr. 50, 760–763.
[15] Vagin, A. and Teplyakov, A. (1997) MOLREP: an automated program for molecular replacement. J. Appl. Crystallogr. 30, 1022–1025.
[16] Herron, J.N., He, X.M., Ballard, D.W., Blier, P.R., Pace, P.E., Bothwell, A.L., Voss Jr., E.W. and Edmundson, A.B. (1991) An autoantibody to single-stranded DNA: comparison of the three-dimensional structures of the unliganded Fab and a deoxynucleotide-Fab complex. Proteins 11, 159–175.
[17] Murshudov, G.N., Vagin, A.A. and Dodson, E.J. (1997) Refinement of macromolecular structures by the maximum-likelihood method. Acta Crystallogr. D: Biol. Crystallogr. 53, 240–255.
[18] Brunger, A.T. (1993) Assessment of phase accuracy by cross validation: the free *R* value. Methods and applications. Acta Crystallogr. D: Biol. Crystallogr. 49, 24–36.
[19] McRee, D.E. (1999) Practical Protein Crystallography, Academic Press, San Diego.
[20] Lamzin, V. and Wilson, K.S. (1997) Automated refinement for protein crystallography. Methods Enzymol. 277, 269–305.
[21] MacCallum, R.M., Martin, A.C. and Thornton, J.M. (1996) Antibody–antigen interactions: contact analysis and binding site topography. J. Mol. Biol. 262, 732–745.
[22] Jones, G., Willett, P., Glen, R.C., Leach, A.R. and Taylor, R. (1997) Development and validation of a genetic algorithm for flexible docking. J. Mol. Biol. 267, 727–748.
[23] Myszka, D.G. (1999) Improving biosensor analysis. J. Mol. Recognit. 12, 279–284.
[24] Stanfield, R.L., Zemla, A., Wilson, I.A. and Rupp, B. (2006) Antibody elbow angles are influenced by their light chain class. J. Mol. Biol. 357, 1566–1574.
[25] Skrabana, R., Skrabanova-Khuebachova, M., Kontsek, P. and Novak, M. (2006) Alzheimer's-disease-associated conformation of intrinsically disordered tau protein studied by intrinsically disordered protein liquid-phase competitive enzyme-linked immunosorbent assay. Anal. Biochem. 359, 230–237.
[26] Khuebachova, M., Verzillo, V., Skrabana, R., Ovecka, M., Vaccaro, P., Panni, S., Bradbury, A. and Novak, M. (2002) Mapping the C terminal epitope of the Alzheimer's disease specific antibody MN423. J. Immunol. Methods 262, 205–215.
[27] Cruickshank, D.W.J. (1996) in: CCP4 Study Weekend. Macromolecular Refinement, pp. 11–22, SERC Daresbury Laboratory, Warrington, UK.
[28] Wilson, A.J.C. (1942) Determination of absolute from relative X-ray intensity data. Nature 150, 151–152.
[29] Ramakrishnan, C. and Ramachandran, G.N. (1965) Stereochemical criteria for polypeptide and protein chain conformations. II. Allowed conformations for a pair of peptide units. Biophys. J. 5, 909–933.
[30] Morris, A.L., MacArthur, M.W., Hutchinson, E.G. and Thornton, J.M. (1992) Stereochemical quality of protein structure coordinates. Proteins 12, 345–364.
[31] Longhi, S., Czjzek, M., Lamzin, V., Nicolas, A. and Cambillau, C. (1997) Atomic resolution (1.0 Å) crystal structure of *Fusarium solani* cutinase: stereochemical analysis. J. Mol. Biol. 268, 779–799.
[32] Sevcik, J., Dauter, Z., Lamzin, V.S. and Wilson, K.S. (1996) Ribonuclease from *Streptomyces aureofaciens* at atomic resolution. Acta Crystallogr. D: Biol. Crystallogr. 52, 327–344.
[33] Walsh, M.A., Schneider, T.R., Sieker, L.C., Dauter, Z., Lamzin, V.S. and Wilson, K.S. (1998) Refinement of triclinic hen egg-white lysozyme at atomic resolution. Acta Crystallogr. D: Biol. Crystallogr. 54, 522–546.
[34] Berriman, J., Serpell, L.C., Oberg, K.A., Fink, A.L., Goedert, M. and Crowther, R.A. (2003) Tau filaments from human brain and from in vitro assembly of recombinant protein show cross-beta structure. Proc. Natl. Acad. Sci. U.S.A. 100, 9034–9048.
[35] Inouye, H., Sharma, D., Goux, W.J. and Kirschner, D.A. (2006) Structure of core domain of fibril-forming PHF/Tau fragments. Biophys. J. 90, 1774–1789.
[36] Mukrasch, M.D., von Bergen, M., Biernat, J., Fischer, D., Griesinger, C., Mandelkow, E. and Zweckstetter, M. (2007) The "jaws" of the tau–microtubule interaction. J. Biol. Chem. 282, 12230–12239.
[37] Ruben, G.C., Iqbal, K., Grundke-Iqbal, I., Wisniewski, H.M., Ciardelli, T.L. and Johnson Jr., J.E. (1991) The microtubule-associated protein tau forms a triple-stranded left-hand helical polymer. J. Biol. Chem. 266, 22019–22027.
[38] von Bergen, M. et al. (2006) The core of tau-paired helical filaments studied by scanning transmission electron microscopy and limited proteolysis. Biochemistry 45, 6446–6457.
[39] von Bergen, M., Friedhoff, P., Biernat, J., Heberle, J., Mandelkow, E.M. and Mandelkow, E. (2000) Assembly of tau protein into Alzheimer paired helical filaments depends on a local sequence motif ((306)VQIVYK(311)) forming beta structure. Proc. Natl. Acad. Sci. U.S.A. 97, 5129–5134.
[40] Kraulis, P.J. (1991) MOLSCRIPT: a program to produce both detailed and schematic plots of protein structures. J. Appl. Crystallogr. 24, 946–950.
[41] Esnouf, R.M. (1999) Further additions to MolScript version 1.4, including reading and contouring of electron-density maps. Acta Crystallogr. D: Biol. Crystallogr. 55, 938–940.
[42] Baker, N.A., Sept, D., Joseph, S., Holst, M.J. and McCammon, J.A. (2001) Electrostatics of nanosystems: application to microtubules and the ribosome. Proc. Natl. Acad. Sci. U.S.A. 98, 10037–10041.